A SuFET Based Sensor for Nano-Microscope

Rostyslav Sklyar

Abstract:

A superconducting field-effect transistor (SuFET) based transducer (sensor) with carbon nanotubes (CNT) or pickup coil kind of input circuit for the nerve and neuron impulses, DNA recombination signals, flows of biochemical molecules, micro- and nanoscopy, and biosusceptibility has been designed. A nanoSuFET with a high-temperature superconducting channel is introduced into the nerve fibre or brain tissue for transducing their signals in both directions. Pickup coils are implanted into an organism in order to obtain the natural or artificially excited biosignals from the organs and tissues. The range of picked up signals varies from 0.6 nA to 10 µA with frequencies from 20 to 2000 Hz. The output signal lies in the range of $(5 \div 5)V$, $(7 \div 0) \cdot 10^{17}/cm^3$ molecules, and $(2 \div 10)$ pH. The sensitivity of this micro- or nanoscope can be estimated as $H_J = 10^{-4}$ $(A \cdot m/\sqrt{Hz})$ with SNR equal to 10^4. The sensitivity of an advanced first-order biogradiometer is equal to $3fT/\sqrt{Hz}$. The smallest resolvable change in magnetic moment detected by this system in the band 10 Hz is 1 fJ/T.

Keywords: *biosignals, SuFET, nanoFET, biosusceptibility, nanoscope, operating conditions*

1. Introduction – Different sensors and diagnostic systems

The sensor converts information or energy from the measurement quantity into another quantity, especially an electrical quantity. This "intermediate" signal may be processed in some way [1]. There are sensor and transducers for electrical quantities especially for current, voltage and magnetic quantities. A biosensor is a device that incorporates a biologically active layer as the recognition element and converts the physical parameters of the biological interaction into a measurable analytical signal [2]. Thanks to advances in nanotechnology, micro-electromechanical systems, molecular diagnostics, and several other technologies, biosensors are now being developed to detect everything from the first chemical signature of cancer to the presence of anthrax.

The technology behind biosensors sounds perfectly simple. Typically, there is a probe on the tip of the sensor that makes contact with blood or tissue. Because of its particular electrical, metallic, and chemical composition, the sensor is able to "react" in a telltale manner when it comes into contact with the target. That reaction is then magnified, quantified, illuminated with various stains and dyes, and then matched against the ever-expanding libraries of gene sequences and protein structures of diseases [3].

There are a number of methods and devices for transducing different biosignals (BSs) into recordable or measurable information. The transfer of nerve impulses (NIs) is the main data flow, which carries sensory information to the brain and control signals from it and the spinal cord to the limbs. That is why detecting currents between neighbouring neurons and ionic currents in the nerve fibres is an important area of research. Electric-field control of physical properties is highly desirable from fundamental and technological viewpoints because it does not introduce any chemical or microscopic structural disorder in the pristine material. This is also the basis of FETs, in which accumulation, depletion, and inversion layers are formed at the interface [4]. Moreover, the complex view on BSs requires further stages of precise processing in order to decode the received or control information.

There are different kinds of transducers/sensors for picking up NIs: room-temperature and superconducting, external and implantable. Development of such devices is increasing the penetration into bioprocess while simultaneously simplifying the exploitation of the measuring systems in order to bring them closer to a wide range of applications. For this reason the magnetometer with a room-temperature pickup coil (PC) (without using the toroidal core) for detecting signals, which can clearly be detected in higher frequency range, was developed in order to simplify the superconducting quantum interference device (SQUID) system. The PC is set outside the cryostat and is connected to the input coil of the SQUID [5] or a channel of superconducting FET (SuFET) [6]. At frequencies higher than 20 Hz the noise decreases as 1/f function and then reaches a high flat noise at 2kHz as 200 fT/√Hz. On the other hand, implantable into nerve fiber transducers are evolving from the ordinary Si-chip microelectronics devices [7] into superconducting and nanodevices [8, 9].

The growing variety of biosensors can be grouped into two categories: implantable and external. Because external sensors employ widely used contact mechanisms like needles and lasers, this branch has advanced faster than implantables. For this reason a working interface between the living tissue of individual neurons and the inorganic compounds of silicon chips were developed. There also was provided the link between ionic channels of the neurons and semiconductor material in a way that neural electrical signals could be passed to the silicon chip. Once there, that signal can be recorded using the chip's transistors. What's more, the neurons can also be stimulated through the capacitors. This is what enables the two-way communications. The project tested the

device by stimulating the neurons and recording which ones fired using standard neuroscience techniques while tracking the signals coming from the chip [10].

The recent achievements in nanoelectronics can be regarded as a further step in the progress of BS transduction. They give us the possibility to create the most advanced and universal device on the basis of known micro systems. Such a sensor/transducer is suitable for picking up BSs- NIs, electrically active (ionised) molecules and the base-pair recognition event in DNA sequences- and transforming it into recognizable information in the form of electric voltage, or a concentration of organic or chemical substances. Moreover, this process can be executed in reverse. Substances and/or voltages influence BSs, thereby controlling or creating them (BSs). Also the new fiber-based optical microfluidic detectors are designed for nano-volume sample measurement. The silicon-glass microdetectors were fabricated by use of micromechanical techniques [11].

The known development of scanning-probe magnetic microscopes is based on circulating Josephson currents in a SQUID loop to produce microwave images with a spacial resolution of about 30 µm [12]. A SQUID-based microwave microscope has some distinct advantages over earlier microwave systems: the spacial resolution is limited only by the size of the SQUID loop. A mice biomagnetic measurement system using a dc SQUID magnetometer for a comparative magnetoencephalogram study of transgenic and wild mice has been developed [13]. A magnetometer with PC of 1.0 mm diameter and 0.7 mm lift-off distance to improve spatial resolution and magnetic field sensitivity was adopted. The magnetocardiogram of a wild mouse was measured as the initial application of the system. The bipolar peak positions in a magnetic field map separated by 5.6 mm were clearly detected with the maximum amplitude of 88 pT.

The advent of semiconductor devices with nanoscale dimensions creates the potential to integrate nanoelectronics and optoelectronic devices with a great variety of biological systems. Moreover, the advances in nanotechnology are opening the way to achieving direct electrical contact of nanoelectronic structures with electrically and electrochemically active subcellular structures-including ion channels, receptors, and transmembrane proteins such as bacteriorhodopsin. Direct electrical interfacing at the biomolecular level opens the possibility of monitoring and controlling critical biological functions and processes in unprecedented ways, and portends a vast array of possibilities such as new classes of prosthetic devices, medical monitoring devices, medical delivery systems, and patient monitoring systems, as well as other applications [14].

2. Sensors and diagnostic instruments: the input signals and flows

Electrical current may be measured by measuring the related magnetic field by means of the Hall effect or the Faraday effect into optoelectronic devices. The measurand as well as the reference value are often converted into quantities of either the same or different physical nature, before they are actually compared with each other [1]. Proceeding from the previously mentioned difficulties, including superconducting element of the sensor/transducer into an electric current could be the solution to the problem. Electronic or ionic currents in conductors or axons respectively, passing through the SuFET's channel induce the output voltage on its gate [8].

Whereas the sensor element can deliver a weak signal, the transmitted signal should generally have a high signal level, and perhaps suitable values, in order to reach superior units undisturbed and to simplify the following calculations. Therefore, the sensor signal should be generally pre-processed. Thereby several important tasks could be realized, such as signal amplification, scaling, linearization, conversion, and conjunction with other components in a chain, parallel, or closed-loop structure [15].

As an electrical signal, the BS has two components: electrical potential or voltage and ionic currents. The first component is sufficiently developed and does not require penetration into the substances of BS propagation. The marketable progress in transducing of the second component began when the necessary instrumentation for measurement of micro and nano dimensions had been created.

The main informational flux from organs of the senses to motor nerves is transmitted through nerve fibres, which consist of a myelin shield with axons as a core. Recent research results suggest that such an arrangement is similar to a transmission line [16]. The nerve impulse in motor nerve of a frog is equal to 2 nA [17]. Synaptic currents between first order neighbouring neurons into *in vivo* or brain slice preparations have an order of 50 pA [18].

The nerve impulses passing through the fibre could be unambiguously defined by detecting the matching ionic current(s) or its superposition. Such a technique seems optimal because even precise voltage measurement could not give a current value according to the Ohm law. First of all, nerve fibre must be separated from a living organism for resistance of fibre measurement and, secondly, this resistance may vary in time. The implantable microelectrodes for neural applications are based on thin-film polymer foils with embedded microelectrodes for both recording and stimulation. Applications for these biomedical micro devices will include stem cell research, cancer cell characterization, drug discovery, treatments for neurological disorders, and neuroprosthetic devices [19].

A. The NIs propagation, measurement and simulation

The signal conducted along the axon is a transient. This difference in potential is the result of ionic gradients due to ionic concentration and is modified by the ionic flow that produces ionic currents. These ionic currents give rise in turn to longitudinal currents closing local ionic current circuits that allow the regeneration of the membrane potential changes in a different region of the axon. This process is a true propagation instead of the conduction phenomenon occurring in wires.
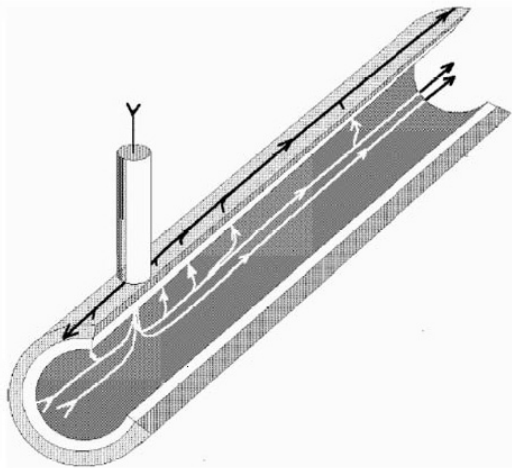
Fig. 1. Longitudinal section of an axon showing a few lines of current flow.

The propagation of the NI in the cylindrical geometry of the axon and the consequences of the geometry of the axon on the current circulation across the membrane and along the axon is show in Fig. 1 [20]. The generation of the action potential has been carried out in an axon with an axial wire.
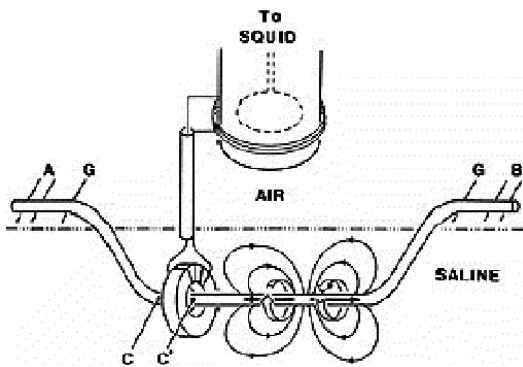

Fig. 2. A nerve action potential propagates from proximal to distal (left to right in the figure).
The wide and narrow arrows around the nerve represent the magnetic and electric field, respectively; the arrows on the nerve axis are equivalent dipole sources.

Fig. 3. The magnetic (solid lines) and electric (dashed lines) signals recorded from a frog sciatic nerve immersed in Ringer solution.

The magnetic fields were recorded with a SQUID magnetometer with a room-temperature PC [21]. At the closest PC-to-nerve separation of 15 mm, the nerve

magnetic field could barely be detected (Fig.2). The magnetic signal is produced predominately by the total axial current i_{bio}, enclosed by the toroid while the voltage action potential in air expresses the charge on the membrane. The magnetic trace should then be proportional to the first derivative of the electric trace, as observed in Fig. 3.
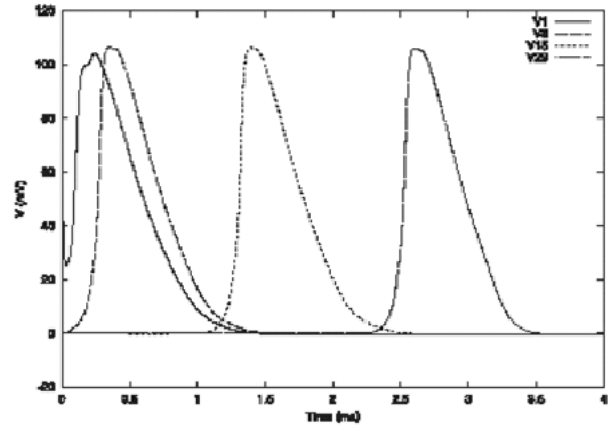

Fig. 4. Test of the single-fiber model. Propagation of action potentials in an isolated normal fiber.

Development of such devices is increasing the penetration into bioprocess while simultaneously simplifying the exploitation of the measuring systems in order to bring them closer to the wide range of applications. Since the field and spatial resolution are highly diminished as the distance between the sample and the sensor increases, the key to this technique is to bring the sensor as close as possible to the sample. The cryogenic positioning system consists of three different main components and is very bulky. SQUID magnetometer systems do not provide the spatial resolution necessary to study the generation of the magnetic activity or injury currents at tissue and cellular scales.

Synchronous impulse transmission and the formation of "condensed" pulse states are found [22]. Electric impulses with a delay of 0.5 ms are presented to the system, and the numerical results show that, for increasing coupling, the impulses tend to adjust their speed and become synchronized (Fig. 4). Cell polarity is critical in various cellular processes ranging from cell migration to asymmetric cell division and axon and dendrite specification. Additionally, Par-3 directly associates and recruits the p75 neurotrophin receptor to the axon-glial junction, forming a complex necessary for myelination. Together, these results point to a critical role in the establishment of cell polarity for myelination [23].

B. Transducing and simulation of the neuron activity

Cultures of neurons can be grown on microelectrode arrays, so that their spike and burst activity can be monitored by a low noise multichannel integrated circuit for recording neuronal signals. These activity patterns are quite sensitive to changes in the environment, such as chemical exposure, and hence the cultures can be used as biosensors [24]. The signalling from the chip through a pair of neurons and back to the chip is thought to be the as a fundamental pathway of future neurochips (Fig. 5)

[25]. The activity of the fundamental element of such future hybrids was recorded by joining a silicon chip with an excitatory chemical synapse between a pair of identified neurons [26].
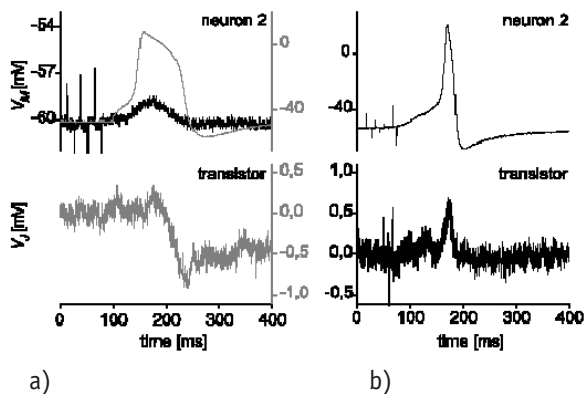

Fig. 5. The neuron-transistor coupling of the postsynaptic neuron:
a) The weak response (noise, left scale) is the postsynaptic response (upper). The strong response is an action potential, right scale (lower). b) Record of microelectrode in neuron (upper). The presynaptic stimulus elicits a postsynaptic action potencial (lower).
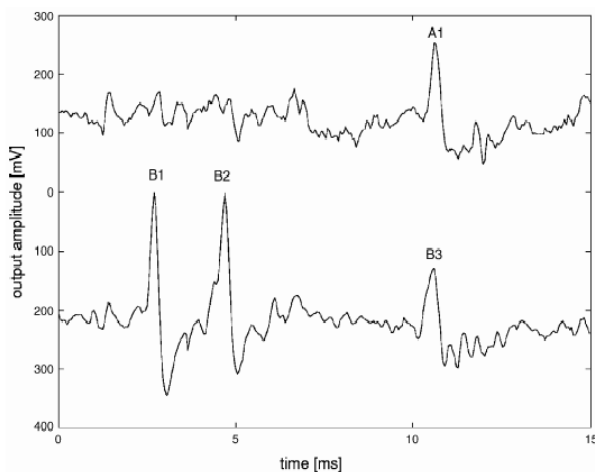

Fig. 6. Analog data from two electrodes recorded simultaneously by the system.
This plot indicates the richness of the information contained in the analog data. The spikes with different amplitudes on the same electrode (B1 and B3) were likely produced by different neurons. The spikes in time coincidence on the two electrodes (A1 and B3) are likely produced by a single neuron.

Modern neurophysiological experiments often require high-density multi-electrode readout systems for recording signals simultaneously from many neurons. Multi-channel readout systems are built mostly in hybrid technologies using off-the-shelf components. With such techniques readout systems with up to several tens of channels have been fabricated [27]. The development described in this paper is driven mainly by a project to readout signals from live retina tissue. Similar readout systems can be used in the study of slices of brain tissue and systems of cultured neurons.

In the experiments with retina, the amplitudes of extra cellular neuronal signals are typically in the range (50–500) µV with the frequency spectrum in the range (20÷2000) Hz (Fig. 6). Both the low signal amplitude and the low frequency range are challenging for an IC design. A low noise preamplifier and proper shaping of the frequency passband are required to optimise the signal-to-noise ratio. In most low frequency applications, high precision switched-capacitor filters play the dominant role.

The nervous system uses two basic types of formats for encoding information. The parameters of many sensory (and some premotor) signals are represented by the pattern of activity among an array of neurons each of which is optimally responsive to a different parameter value [28]. This type of code is commonly referred to as a place code. Motor commands, in contrast, use rate coding: the desired force of a muscle is specified as a monotonic function of the aggregate rate of discharge across all of its motor neurons. Generating movements based on sensory information often requires converting signals from a place code to a rate code.

Sensory maps or place codes are ubiquitous throughout the brain. The individual neurons that make up sensory maps respond maximally to different "preferred" values of the sensory parameter being encoded, and their responses decrease if the actual stimulus either exceeds or falls short of that particular favourite parameter value. Thus, only by examining the responses of a population of such receptors is it possible to deduce what the stimulus actually looks, sounds, feels, smells, or tastes like.
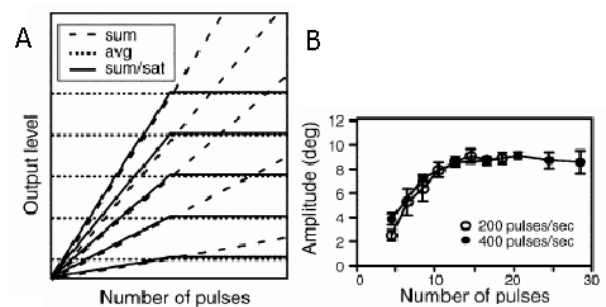

Fig. 7. A simulation of three models, illustrating the relationship between the output and both the location, and the amount of activity:
A - Simulation of the summation, averaging, and summation-saturation models. Each curve represents the output value that occurs for "microstimulation" of a unit at one of five sites in the input map, as a function of the number of pulses of microstimulation delivered to that site;
B - Comparison with actual microstimulation data from the superior colliculus. Microstimulation was conducted at a single site for two different pulse frequencies and for varying durations.

The neural representation of motor commands shares some similarities with sensory systems. To move a body part farther or faster requires a monotonic increase in motor neuron activity. This can occur by increasing the activity level of a given set of motor neurons, by

recruiting additional motor neurons, or both (Fig. 7). The amplitude of the evoked movement initially varies with the number of pulses, then saturates. This behaviour is most similar to the summation-saturation model.
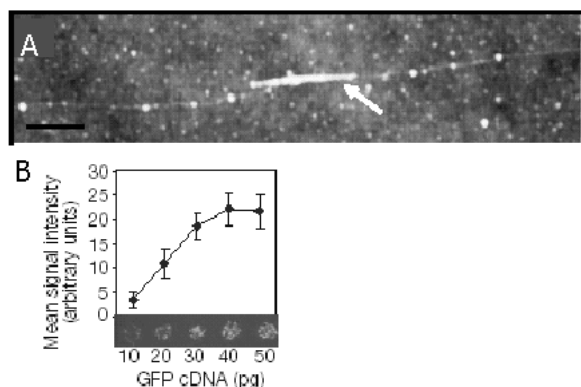

Fig. 8. Genosensor technology.
A - An atomic force microscope image of a 500-base-long (~250 nm) RecA nucleoprotein filament (black arrow) localized at a homologous sequence on λ =DNA scaffold molecule [34];
B - Expression levels of cell clusters in a microarray are propor-tional, over a fourfold range, to the amount of plasmid DNA [35].

The implantable electronic circuits for neural recording and stimulation in freely behaving animals that could provide prosthetic connections to replace or augment damaged pathways in the nervous system have been developing [29]. A Neurochip creates an artificial connection between two sites by using action potentials recorded on one electrode to trigger electrical stimuli delivered to another. The chip made the recordings and stimulations through two implanted electrodes, thus providing a constant connection between the two sites in the brain.

C. Analytical signal of DNA

Recent advances in automated DNA synthesis and the convenient site-specific labelling of synthetic oligonucleotides with suitable functional moieties, coupled with advances in microelectronics, have accelerated the development of biosensors for the analysis of specific gene sequences (Fig. 8). A DNA biosensor (or genosensor) employs an immobilised DNA as the recognition element [2]. Electrochemical DNA biosensors rely on the conversion of the base-pair recognition event into a useful electrical signal. Current DNA detection methods based on sequencing by synthesis rely on optical readouts; however, a direct electrical detection method for this technique is not available. Application of the label-free electrical detection method, charge perturbation detection, applied to sequencing by synthesis, could be used for direct electrical detection of enzymatically catalysed DNA synthesis by induced surface charge perturbation to detect any enzymatic DNA or RNA synthesis as well as other biochemical reactions based on similar principles [30].

D. Non-invasive biomedical instruments

SQUIDs have been a key factor in the development and commercialisation of ultrasensitive electric and magnetic measurement systems. In many cases, SQUID instrumentation offers the ability to make measurements where no other methodology is possible. Although SQUID electronics have the capability to operate well above 1 MHz, most applications tend to be at lower frequencies. Specific examples of input circuits and detection coil configuration for different applications and environments, along with expected performance, are described [31]. In particular, anticipated signal strength, magnetic field environment (applied field and external noise), and cryogenic requirements are discussed. Finally, a variety of applications with specific examples in the areas of electromagnetic, material property, non-destructive test and evaluation, and biomedical measurements are reviewed.

Since the field and spatial resolution are highly diminished as the distance between the sample and the sensor increases, the key to this technique is to bring the sensor, (held in at cryogenic temperatures), as close as possible to the sample. It has been shown that the best combination of spatial resolution and field sensitivity for a specific SQUID geometry occurs when the diameter of the pickup coil is approximately equal to the sample-to-sensor distance [32]. These systems do not provide the spatial resolution necessary to study the generation of the magnetic activity or injury currents at tissue and cellular scales. In excitable tissue extracellular potentials, transmembrane potentials, or action currents are interrelated. The extracellular potentials are typically recorded using microneedles arrays. However, the insertion of microneedles influences the measurement results and is impractical to achieve submillimeter (nano) special resolution. The approach to record the action currents using SQUID microscopy allows us to obtain more detailed information on the generation of the magnetocardiogram (MCG). High-resolution biomagnetic imaging provides insights that will improve existing mathematical models of biological tissue.

3. The components for superconducting nanosensors

CNT-based nanobiosensors may be used to detect DNA sequences in the body. These instruments detect a very specific piece of DNA that may be related to a particular disease. The use of nanotube-based sensors will avoid problems associated with the current much-larger implantable sensors, which can cause inflammation [33]. The devices can be administered transdermally. CNT chemical sensors for liquids can be used for blood analysis (for example, detecting sodium or finding pH value). Implantable sensors can be useful in health assessment. Because of their small size and less power consumption, they are highly suitable as implantable sensors. One way of compensating the loss of photoreceptors is by bypassing the destroyed photoreceptors and artificially stimulating the intact cells in the neighbourhood. Another possible area related to the application of CNTs that can be investigated is cochlear implants related to hearing problems.

Superconducting nanowires are unusual in that they newer show zero resistance, although resistance does exponentially upon cooling [34]. A new class of metallic devices based on DNA molecules is promising due to the self-assembly properties of DNA. As the resistance of the devices is controlled by the spatial profile of superconducting phase within the leads, there is the potential for applications. These include local magnetometry (as is widely done with conventional SQUID) and the imaging of phase profiles created by supercurrents – in essence a superconducting phase gradiometer.

Traditional materials have been pushed to their limits, which means that entirely new materials (such as high-kappa gate dielectrics and metal gate electrodes), and new device structures are required [35]. Entirely new device structures (such as nanowire or molecular devices) and computational paradigms will almost certainly be needed to improve performance. The development of new nanoscale electronic devices and materials places increasingly stringent requirements on metrology.

A. The Available FET's Variants Applicable as SuFET

Application of the SuFET's modifications such as CMOSuFET (low Tc) [36] and coplanar SuFET (high Tc) [37] broadens the range of requirements, which are being satisfied by the SuFET based transducer (SuFETTr). Low-dimensional semiconductor nanostructures and organic molecules, which offer unique possibilities such as extremely low power dissipation, quantum effects, surface sensitivity and low synthesis cost, could be the building blocks for next- generation electronics [38]. Moreover, an organic superconductivity of carbon molecules, known as bucky balls, which can act as superconductors at relatively warm temperatures, raises hopes for loss-free organic electronics and their practical applications in biosensors, including organic ones.
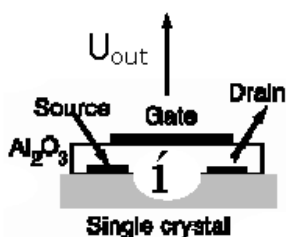
Fig. 9. An organic SuFET device and its electrodes.

High densities of electrons and holes have been induced by gate doping in a FET geometry (Fig. 9). At low temperatures, the material turns superconducting with a maximum transition temperature of 117 K in hole-doped $C_{60}/CHBr_3$ [39]. The increased spacing between the C_{60} molecules increases the density of states, and the resulting increase of T_c is well documented in alkali metaldoped bulk samples (A_3C_{60}). The observation of gate-induced hole doping of C_{60} resulting in a T_c of 52 K suggests that significantly higher T_c's could be anticipated in suitably "expanded" C_{60} crystals. Indeed, here is reported a raise in T_c to 117 K with such methods.
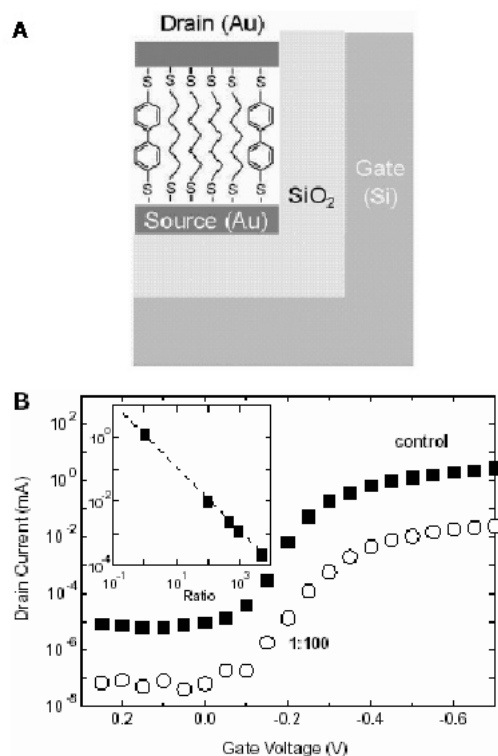
Fig. 10. A - SAMFET structure. A highly doped Si substrate is used as the gate electrode, a thermally grown SiO_2 layer acts as gate insulator, the gold source electrode is deposited by thermal evaporation, and the active semiconducting material is a two-component SAM of alkanedithiols mixed with 4,49-biphenyldithiol or 5,59-terthiophene-dithiol. The drain contact is defined by shallow angle shadow evaporation of gold. The active region of the device is magnified; B - Transfer charac-teristics at room temperature of two SAMFETs (drain-source voltage of 20.5 V). The control corresponds to a "pure" 4,49-biphenyldithiol SAM, whereas the second one is based on a twocomponent SAM (4,49-biphenyldithiol to alkanedithiol ratio is 1:100). The inset shows the current at a gate and drain-source voltage of 20.5 V as a function of the mixture ratio.
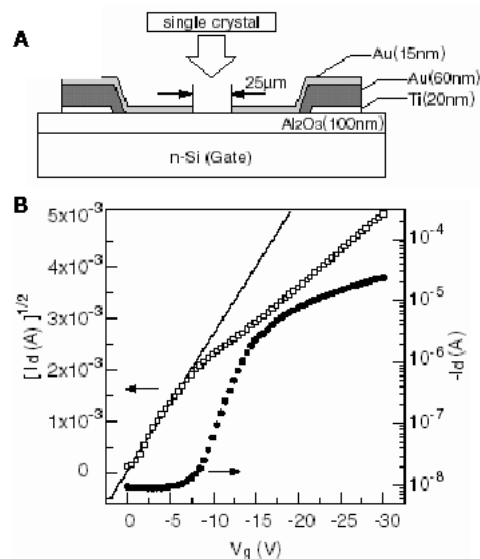
Fig. 11. OFET of organic single cristals with bottom - contact configuration
A - the schematic structure of the fabricated OFET;
B - transfer characteristics of the single cristal FET device at a source-drain voltage Vd of -30 V.

B. Organic FETs with a superconducting potential

Vertical self-assembled monolayer (SAM) FET (SAMFET) action, i.e. conductance modulation through a third electrode, in devices consisting of only several electrically active molecules has been reported [40]. The channel length of 10 to 20 Å is defined by the thickness of a SAM rather than lithography (Fig. 10). Moreover, the peak conductance at low temperatures is quantized in units of $2e^2/h$, indicating that the conductance of single molecules is modulated.

Organic FETs (OFETs) are of great interest for future electrolitic applications due to their flexibility. Up to now, a lot of fabrication processes or device configurations of OFETs have been reported [41]. Most of them were based on thin film technique such as vapour deposition. In general, the thin films for example, amorphous, poly crystalline, polymeric, and so on, consist of grains, and therefore, charge carriers behave as hopping conduction. This decreases the field-effect mobility of devices. Thus, annealing the organic thin films or surface preparations of substrate grows grains, and consequently these devices have few boundaries of grains between source and drain electrodes.
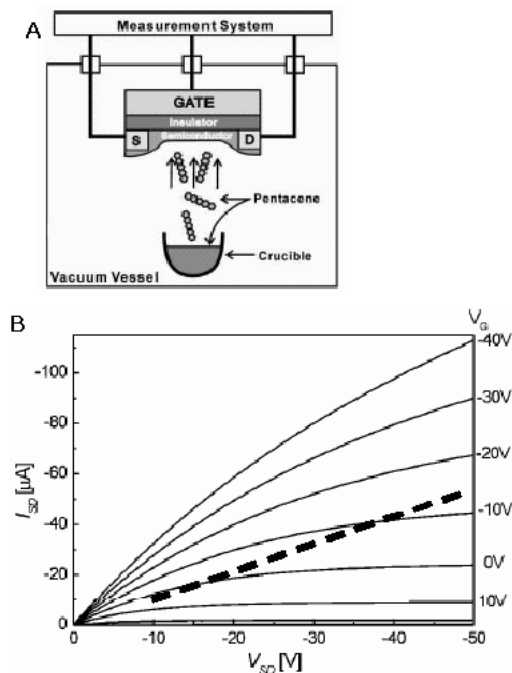

Fig. 12. Thin film (TFT) FET:
A - The source- drain current was measured in situ at various gate voltages;
B - shows channel current (I_{SD}) versus voltage (V_{SD}) for the 20 nm thick pentacene TFT FET.

A quite simple and easy fabrication technique of OFETs with single crystals was proposed, and it demonstrated that the OFETs exhibit high mobility and good device characteristics (Fig. 11). The presented technique makes the fabrication of high performance OFETs easy and serves as a potential way to make organic integrated circuits. Also N-channel and ambipolar OFETs with a few tens of nanometer channel length were fabricated and characterized [42].
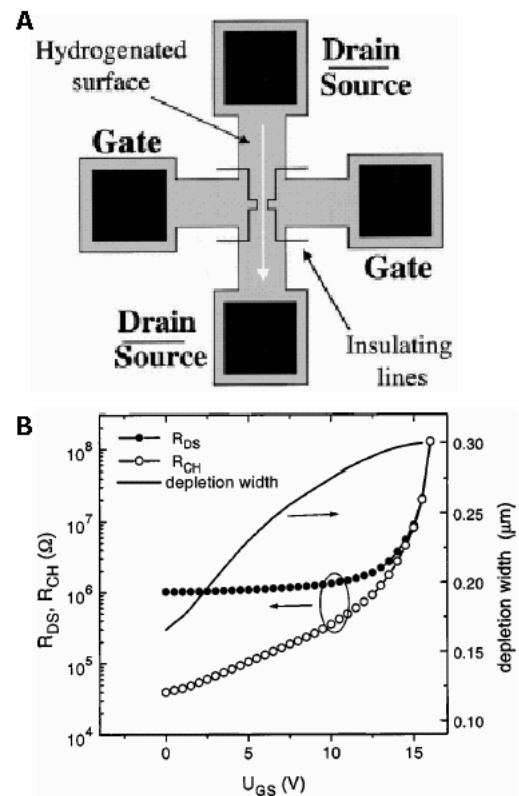

Fig. 13. In-plane gate FET on hydro-genated single-crystal diamond surface:
A - Schematic diagram of an in-plaine FET;
B - Drain-source resistance R_{DS}, channel resistance R_{CH}, and depletion region width as a function of the gate voltage V_{GS}.

A simple but powerful method to observe directly the regions in which the carriers are exhausted or injected by electric fields has been proposed [4]. As shown in the Fig. 12, the source (S)-drain (D) current in thin film transistors (TFT) is measured as a function of the film thickness with a bottom-contact configuration.

The fabrication and characterization of in-plane gate transistors on hydrogenated single-crystal diamond surfaces have been reported [43]. A wire structure is designed in such a way that the gate voltage modulated the conductance of the channel (Fig. 13). The combination of the biocompatibility and tissue equivalence of diamond, as well as the metal-free surface of these in-plane devices, in particular, may open interesting applications for diamond in bioelectronics.

C. NanoFETs with Superconducting CNT Channel (nano SuFETs)

The first such devices were fabricated in 1998. The CNT was simply laid on the gold electrodes and was held by weak van derWaals forces. In addition to increasing the gate capacitance, it is essential that each CNT FET is gated independently by its own gate so that complex integrated circuits can be built [44]. The next generation of CNTFETs with top gates was fabricated by dispersing single-walled (SW) CNTs (SWCNTs) on an oxidized wafer (Fig. 14).

The intrinsic transconductance of CNTFETs in which CNTs were grown by chemical vapour deposition was measured at a drain voltage of -1V was 8.7 mS for a CNT

with a diameter of 1.5 nm (Fig. 15). Estimated intrinsic transconductance was 20 mS when parasitic resistance was taken into account. Measured and intrinsic trans-conductance per unit channel width were 5800 mS/mm and 13000 mS/mm, respectively.
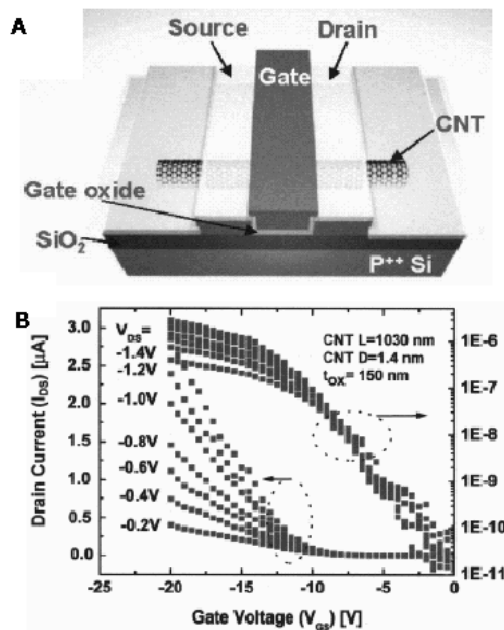

Fig. 14. Schematic representation of top-gated CNTFET:
A - The SWCNT played the role of the "channel," while the two metal electrodes functioned as the "source" and "drain" electrodes. The heavily doped silicon wafer itself was used as the "gate" (back-gate);
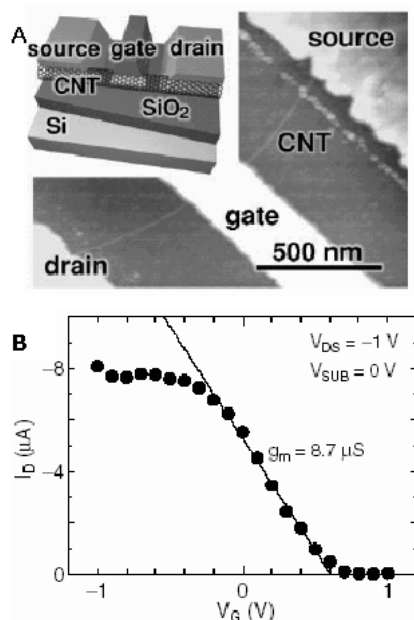B - Transfer characteristics of such a CNTFET.

Fig. 15. CNTFETs with CNTs grown by chemical vapor deposition combined with low-resistance ohmic contacts and top gates:
A - an AFM image of an individual CNT bridging the 1-mm gap between the source and drain electrodes. The gate electrode (LG 210 nm) is formed on the CNT. Inset: Schematic structure of the CNTFET;
B - CNTFET's channel current I_{ds} as a function of V_{GS} at $V_{DS} = -1V$.

This is considerably larger than those for state-of-the-art Si-MOSFETs. This transconductance can be improved drastically by decreasing parasitic resistance and the performance of CNT FETs will advance further by improving the CNT quality and the device structures [45].
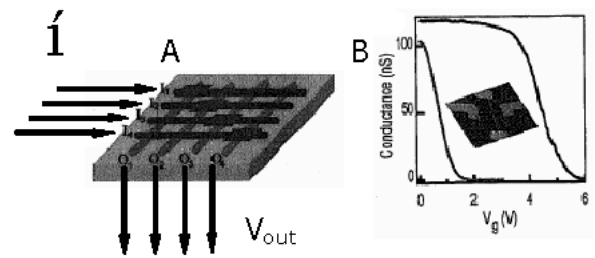

Fig. 16. A 4 by 4 crossed NW-FET array.
A - with four horizontal NWs (I_1 to I_4) as inputs and four vertical NWs (O_1 to O_4) as signal outputs;
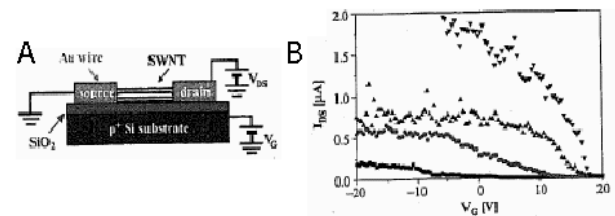B - conductance versus gate voltage of a single cNW-FET.

Fig. 17. A self-assembled SWNT-FET:
A - schematic representation of the electrical measurement circuit;
B - drain-source current versus gate voltage for different values of drain-source bias.

The importance of being able to address nanoscale elements in arrays goes beyond the area of nanocomputing and will be critical to the realization of other integrated nanosystems such as chemical/biological sensors. A regular crossed-nanowire FET (cNW-FET) array (Fig. 16.A) that consists of n-input í and m-output V_{out} n NWs, in which outputs are the active channels of FETs and the inputs function as gate electrodes that turn these output lines on and off [46]. Conductance versus applied NW input gate voltage data (Fig. 16.B) shows that each of the four cNW-FET elements could be turned off with gate voltage of 1V to 2 V, whereas the off-diagonal elements remained unaffected for the same input voltage. When NW are superconducting and, as a result, all cNW-FETs are functioning in SuFET mode, such output voltage V_{out} will show the changes in their conductance.

The realization of a self-assembled SW CNT FET operating at room temperature promotes such strategy as realistic for construction CNT-based electronics (Fig. 17). The assembly process was guided by the information encoded in DNA molecules and homologous genetic recombination [47].

Using a variant of nano-patterning, a self-assembling polymer could also create tiny, finger-shaped silicon protrusions sticking up from the underlying substrate [48]. These fingers would constitute the "channel" in a transistor through which electrons flow- but one in which electrons flow vertically instead of across a chip, as in

today's devices (Fig. 18). The gate to turn the transistor off and on could encircle the silicon finger. The geometry might prevent electrons from "tunneling," or leaking, through the channel when the transistor is in the off state, a constant threat when feature sizes become very small.
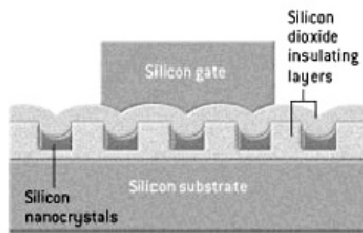

Fig. 18. Self-assembled nanocrystal FET.
A layer of self-assembled silicon nanocrystals is inserted into an otherwise standard device.
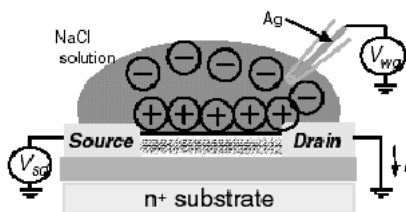

Fig. 19. Schematic of the electrolyte gate measurement.
A water-gate voltage Vwg applied to a silver wire in the pipette is used to establish the electrochemical potential in the electrolyte relative to the device. For -0.9V < V_{wg} < 0.9 V, the leakage current between the water and the Au electrodes/SWNT was negligible (less than 1 nA); the electrolyte then functions as a well-insulated liquid gate.

The excellent device characteristics of SW CNT transistors in salty water also indicate that they may be ideal for biosensing applications. Since a SW CNT has dimensions comparable to typical biomolecules (e.g. DNA, whose width is approximately 2 nm), they should be capable of electrical sensing of single biomolecules [49]. A charged molecule near the SW CNT will act as an effective gate, changing the conductance of the tube. The large transconductances indicate that the signal from single molecules should be readily observable (Fig. 19).

D. The geometry of PC
Since the magnetic biosignals are so small, rejection of all disturbances is of extreme importance. Biological tissues also generate disturbances. The vulnerability to the external magnetic noise can be reduced greatly by a proper design of the flux transformer, which collects the signal and transmit it to the transducer [50]. Two designs, one axial with two oppositely wound superconducting coils, and the other planar of figure-of-eight geometry are insensitive to a spatially uniform background field but respond to changes in an inhomogeneous field as generated by the nearby organ or tissue. To avoid the problems of wire-wound gradiometers, which have only a modest balance, planar integrated sensors offer an elegant solution. The main advantage of flat thin-film gradiometers is their compact structure and

excellent dimensional precision, providing a good intrinsic balance.

The ability to resolve separate sources within the brain or heart should be an important factor for all designs [51]. Different existing instruments can be compared by the dependence of spatial resolving power of the instrument on them. In designing a new system, given the physical constraints of the design, these methods may be used to optimise the system for resolving sources under the experimental conditions anticipated. The vector current sources are the usual equivalent current dipole sources that are the most frequently utilized source models for biomagnetic phenomenon.

The design parameters were the radius (or other geometrical constraints) of the array, the number of sensors, and the spacing of the sensors. Three basic gradiometers are possible [51]. With regards to gradiometer parameters, the type of gradiometer-planar, axial, or normal-and the base line of the gradiometer are important considerations. Finally, the dependence on the sources involves the relative orientation of the sources, the strength of the sources, the number of active sources, and the signal-to-noise ratios (SNR).

An axial first-order gradiometer is formed by coupling the input coil of a flexible high-temperature superconducting flux transformer inductively to a directly coupled SQUID magnetometer [52]. The tape of the transformer is bent such that the two outer pickup loops of the transformer are facing each other while perpendicular to the magnetometer plane resulting in a gradiometer baseline of 35 mm. A superconducting shield is mechanically adjusted to reduce the gradiometer response to uniform fields applied perpendicularly to both the magnetometer plane and the plane of the transformer pickup loops, by a factor of typically 7000.

4. Implantable Sensors:
Design and Performance Data
In general, single sensor systems can only provide partial information on the state of the environment, while multisensor systems combine related data from multiple similar and/or different sensors. The goal of using multisensor systems is to provide synergetic effects that enhance the quality and availability of information about the state of the measurement environment [15].

A number of sensing organs of different physical quantities and environmental conditions are discovered in living beings. On the other hand, output signals from these organs- nerve impulses- can be picked up by state-to-the-art techniques. Further signal processing will define the connection between sensed quantity and output data of such biological sensors. As a result they could be applied in addition to the known artificial sensors for intelligent sensing.

Electrical properties of hybrid structures consisting of arrays of nanowire FETs integrated with the individual axons and dendrites of live mammalian neurons have been reported [53]. Arrays of nanowire-neuron junctions enable simultaneous measurement of the rate, amplitude, and shape of signals propagating along individual axons and dendrites. The configuration of nanowire-axon junctions in arrays, as both inputs and outputs, makes

possible controlled studies of partial to complete inhibition of signal propagation by both local electrical and chemical stimuli. In addition, nanowire-axon junction arrays were integrated and tested at a level of at least 50 "artificial synapses" per neuron.

Interfacing of nerve cells and field-effect transistors is determined by current flow along the electrical resistance of the cell-chip junction [54]. A spectral power density of the junction is $(5 \cdot 10^{-14})V^2/Hz$ and can be interpreted as Nyquist noise of the cell-chip junction with a resistance of 3 MOhm by measuring the fluctuations of extracellular voltage with a low-noise transistor. The thermal noise allows us to elucidate the properties of cell adhesion and it sets a thermodynamical limit for the signal-to-noise ratio of neuroelectronic interfacing.

A. Methods of picking up the biosignals: non-invasive and implantable, electro/magnetic- and biosensors

Voltage potentials of the living organism and its organs are measured by both implantable and external electric field probes of high sensitivity [55]. Information on organ activity is obtained by measuring biomagnetic signals. For such purposes a multi-channel high temperature superconducting interference (high T_c SQUID) system for magnetocardiography (MCG) and magneto-encephalography (MEG) of humans, with high magnetic field resolution has been developed [56, 57].

The known amperometric techniques of biosignals involve the Renview bight realising method [17], and the second method of "biosensors typically rely on an enzyme system which catalytically converts electroche-mically non-active analytes into products which can be oxidized or reduced at a working electrode which is main-tained at a specific potential with respect to a reference electrode" [58]. The same method is applicable also to potentiometic measurements "that can measure substra-tes, inhibitors or modulators of the enzyme". The Renview method requires extra stimulating of the isolated nerve fibre and the other method needs additional reagents and applied voltage. There are two feasible courses for impulse detection. The first one is measuring the magnetic flux around the fibres by PC [59]. The second one is to let the impulses pass through the electronic device with minimal impediments.

B. Devices for matching of biosignal to electronic element (circuit)

Creative integration of microchip technologies and nanostructures is feasible. By tuning the dielectro-phoretic frequency within a microdevice, nanoparticles can be manipulated with the same precision as cells because a one-to-one correspondence exists between a given alternating current frequency and a nanoparticle interaction or biological event. Multiple biological events could be probed simultaneously provided that their corresponding frequencies are distinct. Combined with electroporation, electrokinetics also enables inclusion of molecular complexes inside the cells. Alternatively, functionalized nanoposts can be used to impale cells and relay information from the cell interior to nanoelectronic circuits. By merging the fields of

microfluidics, electrokinetics, and cell biology, microchips are capable of creating tiny, mobile laboratories. The challenge for the future of designing a nano-interface in a microfluidic chip to probe a living cell lies in seamlessly integrating techniques into a robust and versatile, yet reliable, platform [60].

A planar FET can be configured as a sensor by modifying the gate oxide (without gate electrode) with molecular receptors or a selective membrane for the analyte of interest. Binding of a charged species then results in depletion or accumulation of carriers within the transistor structure. An attractive feature of such chemically sensitive FETs is that binding can be monitored by a direct change in conductance or related electrical property, although the sensitivity and potential for integration are limited. The so-called floating gate architecture combines a complementary metal oxide semiconductor (CMOS)-type n-channel FET with an independent sensing area for recording extracellular signals from electrogenic cells was presented [61]. This concept allows the transistor and sensing area to be optimised separately. The noise level of the devices was smaller than of comparable non-metallised gate FETs. The potential of NW nanosensors with direct, highly sensitive real-time detection of chemical and biological species in aqueous solution has been demonstrated [9]. A silicon NW (SiNW) solid state FET, whose conductance is modulated by an applied gate, is transformed into a pH nano-sensor (Fig. 20) by modifying the silicon oxide surface with 3-aminopropyltriethoxysilane (APTES).
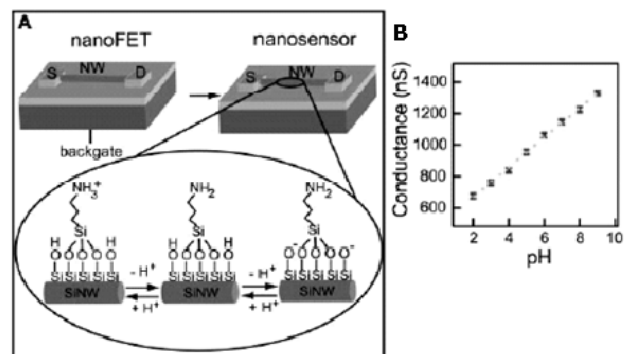

Fig. 20. A pH nanosensor:
A - a silicon NW (SiNW) solid state FET;
B - measurements of conductance as a function of time and solution pH.

The report shows how the scientists fabricate FETs from CNT with the precise electrical properties and any variable band-gap desired. In parallel studies of CNT, researchers have been working to improve the electrical characteristics of individual nanotube transistors [62].

C. Design of a SuFET based either implantable or non-invasive transducer of the BSs

The method of combining the bioelectric nature of NIs and synaptic currents between neighbouring neurons with body-temperature PC and zero resistance input of the SuFET device in order to obtain most advantageous biosensor/transducer was recently advanced [8].

The SuFET is used as a zero-resistance ammeter, which converts drain currents into gate voltages [6].

Transducing the vertical magnetic field from the BSs by the PC that is wrapped around the nerve fibre or DNA sequence is executed similarly to Fig. 2, but the PC is in nano-dimension [63]. By using the said superconducting magnetometer with a room- temperature PC (SIM) [6] it is possible to create the implantable transducer [8].

D. New nano-microscope and biosusceptometer

There was described the eddy current microscopy of thin conducting samples using a SQUID-based magnetic flux microscope in which the sample and SQUID are cooled in liquid nitrogen [64]. If the technique could be extended to the imaging of room temperature samples, it could be used to diagnostic purposes. To achieve a high spacial resolution and flux resolution, this microscope uses a small SQUID directly as a magnetic sensor, rather than a superconducting pickup loop coupled to SQUID. A time-varying field not only induces local eddy currents but also produces currents, which circulate around structures with closed loops. The ability to detect small regions of nonmagnetic conducting materials, and distinguish them from ferromagnets, superconductors, and paramagnets at the microscopic level, gives the magnetic flux microscope broad capabilities in materials analysis. For such testing to be of practical use, it will be necessary to develop systems, which allow the microscopic magnetic imaging of room temperature samples.

In order to realize a short distance between the cooled SQUID and the room temperature sample, a microscope- type SQUID has been developed [65]. In this system, the diameter of the sample is 5 mm. Corresponding to this sample size, a directly coupled thin film gradiometer with two 5×5 mm^2 pickup coils is used, where the gradiometer is chosen to reduce the spatially uniform external noise. The distance between the sample and the SQUID is approximately 1.5 mm, which is short enough for a sample size of 5 mm. The SQUID and the sample are surrounded with three layers of a permalloy magnetic shield in order to reduce the disturbance from the environmental magnetic noise.

A low temperature magnetic susceptometer was constructed by combining an Oxford Instruments Heliox probe sorption pumped 3He cryostat with a Quantum Design model 5000 DC SQUID sensor, giving an effective temperature range from 300 mK to 4.2 K [66]. The smallest resolvable change in magnetic moment detected by this system was found to be Delta~10^{-12} J·T^{-1}.

1) In vivo micro- and nanoscope for scanning and sounding

A new design for scanning or sounding micro- or nanoscopes that combines a simple mechanical arrangement with a miniature SIM's PC. The microwave imaging process (Fig. 21) is shown on a prototype sample: a normal conducting ring of self-inductance L_i and resistance R_i. The quantity L_0 is the PC self-inductance and MI_i represents the magnetic coupling of the PC through a mutual inductance M to an external circuit carrying a current Ii in a tissue [67]. If $\omega_T >> R_i L_i$, then R_i may be ignored and $I_i(\omega_T) \approx -I_j(\omega_T)M/L_i$.
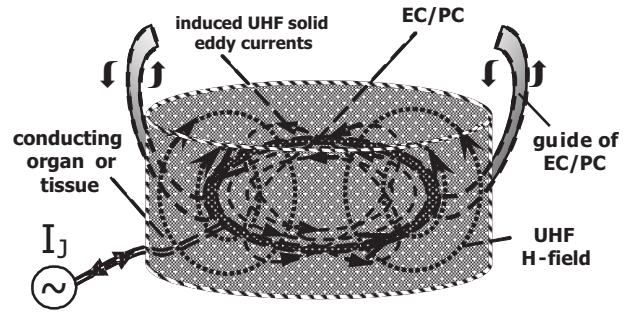

Fig. 21. Schematic diagram of SIM based nano-microscope.

For nonzero drain voltages the SuFET absorbs low-frequency power of the average Josephson current I_J and re-emits this power at extremely high frequencies [6]. When the perturbation is small we can write:

$$I_J(\omega_T) = \frac{2eI_0}{\hbar\omega_T}\left(\frac{V_{DS}}{2} - V_{GS}\right) \tag{1}$$

where

I_o - the critical Josephson current;

V_{DS} and V_{GS} - are the drain-to-source and gate-to-source voltages in SuFET respectively.

ω_T - is closely related to the small signal transconductance of the SuFET.

After defying the factor $K_J = 2eI_0/\hbar\omega_T$ Eq.(1) becomes simple:

$$I_J(\omega_T) = K_J\left(\frac{V_{DS}}{2} - V_{GS}\right) \tag{2}$$

As a result, the decreasing of the SuFET channel's current is defined by the value of losses for eddy currents $I_i(\omega_T)$ in the tissue:

$$\tag{3}$$

$$\Delta I_J(\omega_T) = I_J(\omega_T) - I_i(\omega_T) = K_J\left(\frac{V_{DS}}{2} - V_{GS}\right)\left(1 - \frac{M}{L_i}\right)$$

Thus, by monitoring the change in $\Delta I_J(\omega_T)$ as a function of PC position, we make use of the factor M/L_i dynamics of the tissue to obtain a micro- or nanowave-screening image.

Because I_J flows around the SIM's PC(s), it produces a time varying MF in the envelope of the PC(s) which can serve as a local probing field (Fig. 21). By adjusting I_J, one can continuously adjust the magnetic field. To achieve a high spatial resolution, our nano-microscope uses a small ambient temperature PC(s) directly as a magnetic sensor, rather than a SQUID's pickup loop coupled to a cooled SuFET. Sounding and scanning closer to the tissue improves the spatial resolution, thanks to the complete penetration into the measuring process. Other than the SuFET itself, there are no other microwave components, sources, or detectors. This is particular advantageous at very high frequencies where components are difficult to construct. In conclusion, we note that the ability to detect small regions of nonmagnetic

conducting materials, gives the magnetic flux nano-microscope broad capabilities in material analysis. Since the developed system allows the micro- and nanoscopic of room and tissue temperature samples, such testing will be of practical use for clinical diagnostic.

The sensitivity of this instrument H_J can be estimated by considering the noise source I_{NJ} of SuFET according to Ref. [6]. The digital value of H_J for PC with the diameter of 0.1 μH and inductance 1 μH, and $I_{NJ} = 10^{-11}$ (A·Hz) is equal to: $H_J = I_{NJ}L/\mu_0 S_{eq} = 10^{-4}$ (A·m/√Hz). This means that with a SIM exciting signal $H_{sign} = (V_{DS}/2-V_{GS})/$ $/\mu_0 S_{eq}\omega_T = (V_{DS}/2-V_{GS})\cdot 10^3 \approx 1$ (A·m) a magnetic SNR in a band less than 10 Hz will be: $H_{sign}/H_R(\Delta 10Hz) =$ $= (V_{DS}/2-V_{GS})/ I_{NJ}L\omega_T$. For the said values, SNR of the described nano-microscope will be equal to $H_{SNR} =$ $= (V_{DS}/2-V_{GS})\cdot 10^7 \approx 10^4$. Typically our magnetic images are taken at about 8 pixels/s.

2) In vivo biosusceptometer of organs and tissues

There are several commercial SQUID biosuscepto-meters available [68]. They have been specially designed for high-sensitivity measurements on small HTS samples at very small fields (below 1 mT) in the temperature range from 4.2 K to room temperature. When operated in AC mode the magnetometer measures the real and imaginary components of the AC susceptibility. Note that without the ability to make highly sensitive AC measurements, it would not be otherwise possible to distinguish between intrinsic and defect determined properties. In the AC mode the noise-limited sensitivity was estimated from measurements on a niobium foil of known mass to be $10^{-12} \cdot$ Am^2 √Hz.

A technique had been previously developed, based on magnetic field measurements using a SQUID sensor, to localize in three dimensions steel needles lost in the human body. In all six cases that were treated until now, the technique allowed easy surgical localization of the needles with high accuracy. Despite the importance of needle localization, the most prevalent foreign body in the modern society is the firearm projectile (bullet), generally composed of lead, a paramagnetic material, thus not presenting a remnant magnetic field as steel needles do. On the other hand, since lead is a good conductor, eddy current detection techniques can be employed, by applying an alternating magnetic field with the aid of excitation coils. The primary field induces eddy currents on the lead, which in turn generate a secondary magnetic field that can be detected by a magnetometer, and give information about position and volume of the conducting foreign body. A theoretical study for the development of a localization technique for lead bullets inside the human body was presented [69].

The main difficulties in the measurement of biosus-ceptibility are irregular shapes of the investigated objects, which are difficult to be formalized, and this susceptibility is inhomogeneous. Following, the measu-rement *in vivo*, the PC should be maximally penetrative and flexible to follow the object's form and miniature to have the high-resolution ability. Simultaneously, the angle between the outside- magnetized coil- and an inside PC should be adjusted due to the amplification of the signal from some particular area. Also to raise the

sensitivity to deeply, laid down *in vivo* areas, it is necessary to use the Helmholtz coils for the creation of the laminar magnetic fields.
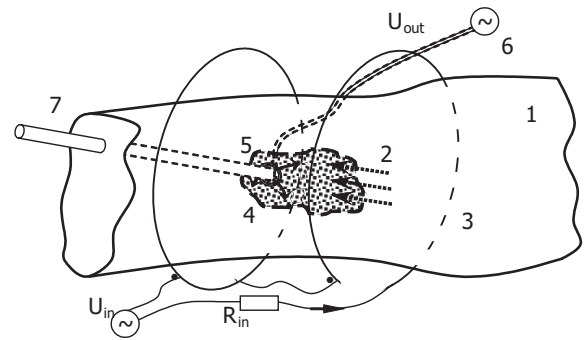

Fig. 22. A simplified circuit for a SIM based biosusce-ptometer.

Taking into account all the described requirements it is advancing the configuration of the measuring system that shown in Fig. 22. The part of living object 1 is excited by a quasi DC or AC magnetic field H(r) 2, generated by Helmholtz coils 3, is penetrated into the investigating subject 4. The magnetization M(r) of an organ or tissue 4 is detected by the *in vivo* PC 5 of SIM 6 that creates a corresponding output voltage U_{out}. PC has been handling in any direction of the subject's irregular form by a biochemically inert rod or manipulator 7.

For the biological tissues the magnetization M(r) in the point r is defined by the value of magnetic susceptibility $\chi(r)$ as:

$$M(r) = \chi(r) \cdot H(r) \qquad (4)$$

where H(r) is defined by the supplied current I_{HI} and the transforming factor of the coils K_{HI} as: $H(r) = K_{HI} \cdot$ $\cdot I_{HI} = H(r) = U_{in}K_{HI}/R_{in}$. The value of M(r) with the frequency f and energy resolution of SuFET E_J will be defined as [6]:

$$M(r) = \frac{eI_0 V_{GS} z_c}{\pi \mu_0 S_{eq} E_J \omega_T f} \qquad (5)$$

where
z_C - the impedance of PC;
μ_0 - the permeability of free space, $\mu_0 = 4 \cdot 10^{-7}$ henry/meter;
$E_J = 10^{-30}$ (J/Hz);
S_{eq} - equivalent area of PC.

From Eq. (4) and Eq. (5):

$$\chi(r) = \frac{eI_0 V_{GS} z_c R_{in}}{\pi \mu_0 S_{eq} E_J \omega_T U_{in} K_{Hl} f} \qquad (6)$$

If we define $K_\chi = \dfrac{eI_0 z_c R_{in}}{\pi \mu_0 S_{eq} E_J \omega_T K_{Hl}}$

as a factor of biosusceptibilitymeter, the value of $\chi(r)$ will be calculated simple:

$$\chi(r) = K_\chi V_{GS}/U_{in} \qquad (7)$$

$\chi(r) = K_\chi V_{GS}/U_{in} f$. For the said values of the SIM's circuit, $K_{Hl} = 10(m^{-1})$, and exiting frequency 10 Hz, $\chi(r)$ will be equal to $\chi(r) = 5 \cdot 10^4 \cdot V_{GS}/U_{in}$.

The shape of PC(s) should be designed according to the specific conditions and aims of the BM measurements. These PCs can be as gradiometer of different order [51], also with the compensation coils [59]. The biogradiometer of first with the coils of an equal area has a factor of efficiency $\eta = 2$ and for a second order- $\eta = 6$.

For the typical reference of a PC's radius to the radius of wire as the value of $a/c = 10^2$, the previous sensitivity of biogradiometer is defined as: $S_H = 4 \cdot 10^{-6} \eta E_J/a^3$. For the PC's radius 0.001 (m) the sensitivity of an advanced first-order biogradiometer is equal to: $3fT/\sqrt{Hz}$. The smallest resolvable change in magnetic moment detected by this system in the band 10 Hz is: $(E_J/S_H =) 1 fJ/T$.

The sensitivity of this biosusceptibilitymeter can be increased by using of PCs as gradiometers of a second and high order (with $\eta = 6$ and more). As a result, it appears the possibility to refuse both of the shielding room and cryogenic system for PC(s). At the same time, the design of *in vivo* PS(s) varying from nano-micro dimensions to the large shapes of conducting material, which are assembled around the functioning organs, or regions of the living tissue has been under investigation.

5. Connection of Su(CNT)FETs with the BS's medium

Microdevices with electroplated wire traces were etched with well-defined edges. These devices are implanted in living bodies to connect nerve tissue with electronics to record nerve cell activities or restore lost functions by stimulation of nerve cells. Electroplating of gold meets the requirements for producing neural implants with low-ohmic wire traces, because this technique allows the microfabrication of gold layers with a thickness of several micrometers and lateral dimensions in the same range. Hence the mechanical stability of the electroplated gold is sufficient for chronic implantation of the structures [70]. The implantable microelectrodes for neural applications are based on thin-film polymer foils with embedded microelectrodes for both recording and stimulation [71].

Very efficient attachment mechanisms are those in which patterned surface structures interact with the profile of the substrate. This general trend is quantitatively explained by applying the principles of contact mechanics, according to which splitting up the contact into finer subcontacts increases adhesion. This principle is widespread in the design of natural adhesive systems and may also be transferred into practical applications [72].

Recently, strong evidence has been presented that the adhesion of gecko setae is caused by van der Waals interaction, rejecting mechanisms relying on capillary adhesion. Elements of contact mechanics have also been applied to this problem and it was predicted that arrays with smaller setae endings should result in greater adhesive strength. An extensive microscopical study of biological surface devices has been combined with the theory of contact mechanics based on molecular adhesion.

The creation of a permissive environment for axonal regrowth was described using a synthetic biological nanomaterial that self assembles *in vivo*, with components that break down into beneficial building blocks and produce no adverse effects on the nerve fibre. This discovery, by reducing or overcoming the first two obstacles and possibly more, allows for the reconnection of disconnected parts of the nerve fibre [73]. Thin films of carbon nanotubes deposited on transparent plastic can serve as a surface on which cells can grow and these nanotube films could potentially serve as an electrical interface between living tissue and prosthetic devices or biomedical instruments. Both cell types were placed on ten-layer-thick "mats" of single-walled carbon nanotubes (SWNTs) deposited on transparent plastic. This enabled to use a microscope to position a tiny electrode next to individual cells and record their responses to electrical pulses transmitted through the SWNTs [74].

6. The main arrangements of SuFETTrs

Among the variety of the above-presented FET devices there are majority of them, mainly modifications of nanoFETs, which allow simultaneous processing of a number of BSs directly or from the PC [8]. There are two factors that make simultaneous processing possible. First of all, the sizes of nanoFETs and nanoPCs are in the same order as the transmitting substances of BSs, such as axons, neurons, and the DNA spiral. Secondly, the cNW-FET array (Fig. 16) is, in itself, multi-input.

The remaining part of FET devices is applicable for serial connection to the said mediums. In addition, some of these FETs can be arranged in the chain in order to transduce the BSs into different physical and chemical quantities and vice versa.

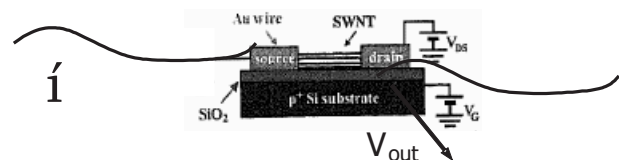### A. Serial Connection of BSs to SuFETTr

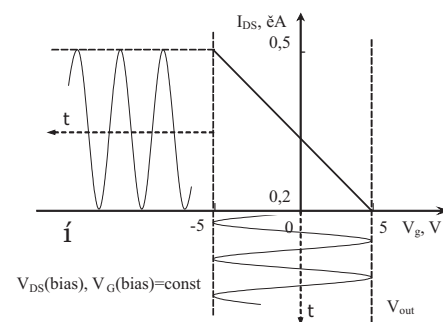*Fig. 23. Schematic of SuFETTr in the serial connection.*

Fig. 24. Operational pattern of a serial SuFETTr.

The organic or nano SuFET device shown, for example in Fig. 17, is connected with the source of BSs through the said micro or nano contacts according to Fig. 23. In such case the current of í, passing through the SuFET's

channel arouses Vout on the gate with some constant bias voltages V_{DS}, V_G (Fig. 24). Transfer function (TF) of the device defined by its numerical order as follows:

$$K_{DNA} = \frac{V_{out}}{i} \Rightarrow \left[\frac{10}{0,5\mu A}\right] = 2 \cdot 10^7 \left[\frac{B}{A}\right] \qquad (8)$$

As the channel of the majority of cited FETs is not superconducting in the present stage of development, it is possible to define the sensitivity threshold (ST) by the channel's resistance R:

$$U_{noise}^{DNA} = \sqrt{4kTR} \qquad (9)$$

where
k - the Boltzmann constant,
T - absolute temperature of FET's channel.

The noise voltage of SuFETs is obtained analogous to the Johnson noise value for the resistive circuit as [6]:

$$(E_N)^2 = 4kT_{SuFET}\gamma_{noise}/g_{dn} \quad \text{and} \quad g_{dn} = I_0/V_C \qquad (10)$$

where γ_{noise} is the ratio of the kinetic energy of the JJ link to thermal energy and V_C -characteristic voltage. Ratio γ_{noise} is proportional to the normalized gate charge g_G/C (g_G is the total gate charge reflected in the channel).

The peak currents range of BS from 5 to 10 µA [21] give a maximal output voltage V_{out} on absciss axis -5 to 5 V also with the necessity of some its reducing it slightly by changing V_{DS}(bias) of the FET's channel. A current, which elicits an action potential in the neuron, is 0.6 nA [25] and will stimulate V_{out} of the transducer equal to 12 mV.

B. Parallel Connection of BSs to SuFETTr

An example of connecting the axons of nerve fibre to multi-input cNW-FET [46] array is shown in Fig. 25. The output voltage of the transducer according to Fig. 16.B lies in the range of 1 V (linear part of the curves).
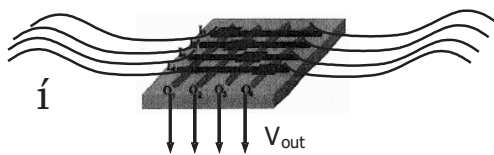

Fig. 25. Schematic of SuFETTr in the parallel connection.
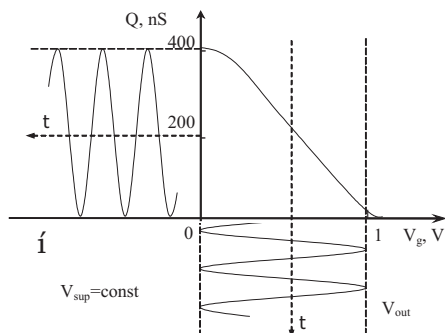

Fig. 26. Operational pattern of a parallel SuFETTr.

The operational pattern of the transducer for one input BS into cNW-FET is shown in Fig. 26. The input BS changes conductance of the FET's channel which influences output voltage V_g.

TF of this device will be similar to the previous one:

$$K_{cNW} = \frac{V_{out}}{V_{sup}Q + i} \Rightarrow \left[\frac{1B}{10^{-7}A}\right] \cong 10^7 \left[\frac{B}{A}\right] \qquad (11)$$

Similarly the value of V_{out} can be obtained for organic, chemical and DNA SuFETTrs.

The carrier density thus obtained is a function of the distance x from the interface (Fig. 11). The large carrier density at $V_G = 0$ V in small x region is due to the charge transfer from the Au electrodes to the pentacene molecules [4]. Carrier density n(x) is a function of the distance (x) from the interface at various gate voltages (V_G). According to the Eq.(4) deviation of carrier density n(x) in the range of maximal $V_{out} = \pm 15$ V is equal to $(7 \div 0) \cdot 10^{17}/cm^3$.

Chemical SuFETTr converts the changes in pH through Q of the channel (similarly to pH nanosensor Fig. 20.A [9]) also into output signal V_{out}. In the scale of Q from 10 to 400 nS a pH (2 to 10) is transformed into variations of V_{out} from 0 to 1 V (Fig. 26).

The potential applied during immobilisation of thiol-modified DNA lies in a different potential window from -0.7 to +0.7 V [2]. The corresponding current í=$V_{in}Q$, to this voltage which is put into the FET channel, according to Fig. 26 vary from 0.4 to 1.8 nA.

Clean gold monolayers are stable in the potential range from -400 to +1400 mV in dilute sulfuric acid solutions, thus allowing electrochemical applications. The careful selection of the terminal functionalities of the monolayers and the proper surface chemistry allows a tremendous flexibility in biosensor design.

ST of the biosensor/transducer in the first approximation (generally) depends on the conductance Q of the superconducting channel. An absolute sensitivity of the transducer with n parallel inputs in the said frequency range derives also from the Johnson noise:

$$U_{noise}^{cNW} = n\sqrt{4kT/Q} \qquad (12)$$

which for cNW-FET varies in the range 50 to 150 nS [46] and gives the order of ST 10^{-7} V/√Hz. Also for the noise voltage of parallel SuFETs based transducer is:

$$(E_N)^2(n) = 4nkT_{SuFET}\gamma_{noise}/g_{dn} \qquad (13)$$

7. Results

Application variety of the novel superconducting, organic and CNT FETs allows us to design transducers of BSs (electronic, nerve, DNA, etc.) that transduce them into different quantities, including electric voltage, density of chemical and biomolecules. On the other hand, the said BSs can be controlled by the applied electrical signals, or bio and chemical mediums.

The described SuFETTrs designed on the basis of organic and nano SuFETs are suitable for describing the wide range of BS dynamical parameters (see Table 1).

Following the columns of the table, it should be noticeable, that serial connection of the external PCs allows us to gain some integrated signal, i.e., the whole sensing or control electronic or NI, which spreads along the number of axons of the nerve fibre; the amount of ions passing through the PCs and the generalized BS passing through one or both spirals of DNA. When SuFET channel(s) of are implanted into the tissue or process we can acquire more precise data about the frequency distribution of NIs, volume distribution of ionized molecules and detecting activity of individual nucleoteds.

Table 1. Dependence of the received BS parameters on the mode of SuFETTr's functioning.

Mode Medium	Serial		Parallel	
	external	implantable	external	implantable
Current	$\int i=1$ cont. or sens. imp.	$i=i(f_1)+i(f_2)+...+i(f_N)$	di/dt, di/dx	$\sum i=1$ network or 1 fibre
Molecules	$\int$ BSs→bio and chem. molec.	variation of BSs→ concentr. of molec.	$\sum$ BSs=1 type of molec.	$\sum$ BSs=$\sum$ bio and chem. molec.
DNA	propagation of BS along DNA's spirals	decoding the BSs of nucleoted recognition	space and lengh dynamic on both spirals	4 nucleoteds→ 4 outputs

The described biosusceptometer or nano-microscope designed on the basis of SuFETTrs is suitable for investigating both the structure of organic objects and their comparing analysis (see Table 2). Following the strings of the table, it should be noticeable, that investigations of biological surfaces are performing according to the surface integrals for a biosusceptometer and nano-microscope modulus respectively. The surface gradients are acquiring by finding of the difference between the respective values of I_1 or I_2. The same is applying to the investigations of biological volumes V_1 and V_2 as the double and triple integrals respectively. The next two strings are explaining the bounds on the possible spreading of the said method.

Table 2. Dependence of the received structure parameters on the mode of functioning- a biosusceptometer or nano-microscope.

Mode Medium	biosusceptometer modulus	nano-microscope modulus	biosusceptometer gradient	nano-microscope gradient
Surface	$I_1=\iint_S f(x, y, z)ds$	$I_2=\iint_S f(x, y, z)dxdy$	$\Delta I_1=I_1'-I_1''$	$\Delta I_2=I_2'-I_2''$
Volume	$V_1=\iint_S f(x, y)dxdy$	$V_2=\iiint_V f(x, y, z)dv$	$\Delta V_1=V_1'-V_1''$	$\Delta V_2=V_2'-V_2''$
Structule level	Investigation of sheath (envelopes) of organs	Investigation of the inside structure of the organs and tissues	Comparing investigation of the organ's or tissue's areas	Differential investigation the twin (pair) organs or tissues
Object (body) level	Investigation of homogeneous organs or tissues	Investigation of inhomogeneous organs or tissues	Comparing investigation of the homogeneous organ's or tissue's areas	Differential investigation the inhomogeneous twin (pair) organs or tissues

Exploitation of the parallel input to SuFETTr allows determination of space and time dynamics of BSs in the nerve fibre and DNA spiral(s) and also the amplification of output signal U_{out} by multiplying the concentration of molecules according to a number of input BSs. After the implantation of parallel SuFET(s), the averaging or summation of this dynamic among the whole neural network, nerve fibre or DNA spiral(s) is possible.

8. Conclusions

The invented biotransducer has the following fundamental improvements upon existing ones:

a) the sign of the output voltage permits the determination of the direction of the input bioflow passing through a single SuFET device;

b) situating the reference electrode outside the living organism makes precise measurement possible;

c) the capability to regulate the proportion of axons, neurons or flows that are being investigated to the untouched ones- either the whole cross section of the fibre or flow, or any part of them;

d) the possibility to substitute the SuFET device or to adjust its ratings to comply with the conditions of the measurement process without repeatedly destroying nerve fibre or flow vessel;

e) the transducer could create conversion in both directions, respectively in passive and active modes;

f) the combination of biocompatibility and tissue equivalence in both the diamond and protein-based (organic) FETs makes them naturally fit for implantation;

g) the possibility to compose a converging device by changing the instrument - from a current sensor to biosusceptometer, from a flowmeter to nano-microscope, etc. - by switching-over (modifying) of SuFET's working mode or transferring from the natural ambient conditions to applying of the exciting magnetic field.

The reviewed variety of FETs shows the varying extent of readiness for them to be exploited them in SuFETTr of BSs. The most appropriate for such an application are the ordinary solid-state SuFET modifications and novel CNT based SuFETs. The organic SuFETs are not amply developed, but this work is being carried out in a number of directions. At the same time, the PCs, which are necessary for the external sensor with respect to the transducing medium (solid-state conductor, nerve fibre, flow of ions and DNA spiral), and corresponding low-ohmic wire traces for connecting PCs to the FET's channel are sufficiently developed, even at nano dimensions.

The preliminary calculations confirm the possibility of broadening the SuFETTr's action from magnetic field to the biochemical medium of BSs. The main parameters of such BSs can be gained by applying the arrangement of the SuFETTr(s) to the whole measurement system. Two directions of SuFETTr function enable decoding of the BS by comparing the result of its action on some process or organ with an action on them of the simulated electrical or biochemical signal after their reverse transducing through the SuFETTr(s). Furthermore, this decoded signal will provide a basis for creating feedback and feedforward loops in the measuring system for more precise and complete influence on the biochemical process.

AUTHOR

Rostyslav Sklyar – Independent researcher, Verchratskogo st. 15-1, Lviv 79010 UKRAINE; tel./fax: +380 322 762432/769613, e-mail: sklyar@tsp.lviv.ua.

References

[1] Weiss H., "Electrical measurement and instrumentations - today and tomorrow", *Measurement*, 1993, no. 12, pp. 191-210.

[2] Lucarelli F., Marrazza G., Turner A. P. F. *et al.*, "Carbon and gold electrodes as electrochemical transducers for DNA hybridisation sensors" (Review), *Biosensors and Bioelectronics*, 2004, no. 19, pp. 515-530.

[3] S. Herrera, *I've got you under my skin, Red Herring*, 2003. Available at: http://www.redherring.com/insider/2003/02/biosensors020503.html.

[4] M. Kiguchi, M. Nakayama, K. Fujiwara *et al.*, "Accumulation and Depletion Layer Thicknesses in Organic Field Effect Transistors", *Jpn. J. Appl. Phys.*, 2003, vol. 42, Pt. 2, issue 12A, L1408-L1410.

[5] A. Kandori, D. Suzuki, K. Yokosawa *et al.*, "A Superconducting Quantum Interference Device Magnetometer with a Room-Temperature Pickup Coil for Measuring Impedance Magnetocardiograms", *Jpn. J. Appl. Phys.*, 2002, vol. 41, Pt. 1, pp. 596-599.

[6] R. Sklyar, "Superconducting Induction Magnetometer", *IEEE Sensors J.*, 2006, no. 6, pp. 357- 364.

[7] P. Fromherz, "Electrical Interfacing of Nerve Cells and Semiconductor Chips", *CHEMPHYSCHEM*, 2002, no. 3, pp. 276-284.

[8] R. Sklyar, "A SuFET Based Either Implantable or Non-Invasive (Bio)Transducer of Nerve Impulses", *Proceedings of the 13th International Symposium on Measurement and Control in Robotics - ISMCR'03*, Madrid, Spain 2003, pp. 121-126.

[9] Y. Cui, Q. Wei, H. Park *et al.*, "Nanowire Nanosensors for Highly Sensitive and Selective Detection of Biological and Chemical Species", *Science*, 2001, no. 293, pp. 1289-1292.

[10] P. Fromherz, Vassanelli S., and Greeff N. G., *NACHIP Project*, Reference: IST-2001-38915, 2006. Available at: http://www.biochem.mpg.de/mnphys/europroject/project.html.

[11] S. Bargiel, A. Górecka-Drzazga, J. A. Dziubana *et al.*, "Nanoliter detectors for flow systems", *Sens. Act. A*, 2004, no. 115, pp. 245-251.

[12] R. C. Black, F. C. Wellstood, E. Dantsker *et al.*, Microwave Microscopy Using a Superconducting Quantum Interference Device", *Applied Physics Letters*, 1995, no. 66, pp. 99-101.

[13] Y. Ono, A Ishiyama, "Development of biomagnetic measurement system for mice with high spatial resolution", *Applied Physics Letters*, 2004, no. 85, pp. 332-334.

[14] M. A. Stroscio, M. Dutta, "Integrated biological-semiconductor devices", *Proc. IEEE*, 2005, no. 93, pp. 1772-1783.

[15] O. Kanoun, H.-R. Tränkler, "Sensor Technology Advances and Future Trends", *IEEE Trans. Instrum. Meas.*, 2004, no. 53, pp. 1497-1501.

[16] C. Hanisch, "Nervensache", *Bild der Wissenschaft*, 1999, no. 2, pp. 70-74.

[17] I. Tasaki, *Nervous transmission*, Charles C. Thomas Publ., Springfield IL USA, 1953.

[18] C. Wyart *et al.*, "Constrained synaptic connectivity in functional mammalian neuronal networks grown on patterned surfaces", *Journal of Neuroscience Methods*, 2002, no. 117, pp. 123-131.

[19] K. C. Cheunga, Ph. Renaudb, "BioMEMS for medicine: On-chip cell characterization and implantable microelectrodes", *Solid-State Electronics*, 2006, no. 50, pp. 551-557.

[20] F. Bezanilla, *The Nerve Impulse*, 2004. Available at: http://pb010.anes.ucla.edu.

[21] J. P. Wikswo, J. P. Barach, and J.A. Freeman, "Magnetic Field of a Nerve Impulse: First Measurements", *Science*, 1980, no. 208, pp. 53-55.

[22] S. Reutskiy, E. Rossoni, and B. Tirozzi, "Conduction in bundles of demyelinated nerve fibers: computer simulation", *Biol. Cybern.*, 2003, no. 89, pp. 439-448.

[23] J. R. Chan, Ch. Jolicoeur, J. Yamauchi, "The Polarity Pro-tein Par-3 Directly Interacts with p75NTR to Regulate Myelination", *Science*, 2006, no. 314, pp. 832-836.

[24] J. J. Pancrazioa, G. W. Gross, "Measuring synchronization in neuronal networks for biosensor applications", *Biosensors and Bioelectronics*, 2004, no. 19, pp. 675-683.

[25] M. Jenkner, B. Muller, and P. Fromherz, "Interfacing a silicon chip to pairs of snail neurons connected by electrical synapses", *Biol. Cybern.*, 2001, no. 84, pp. 239-249.

[26] R. A. Kaul, N. I. Syed, and P. Fromherz, "Neuron-Semiconductor Chip with Chemical Synapse between Identified Neurons", *Phys. Rev. Lett.*, 2004, no. 92, 038102 (4 pages).

[27] W. Dąbrowski, P. Grybos, and A. M. Litke, "A low noise multichannel integrated circuit for recording neuronal signals using microelectrode arrays", *Biosensors and Bioelectronics*, 2004, no.19, pp. 749-761.

[28] J. M. Groh, "Converting neural signals from place codes to rate codes", *Biol. Cybern.*, 2001, no. 85, pp. 159-165.

[29] A. Jackson, J. Mavoori, E. E. Fetz, "Long-term motor cortex plasticity induced by an electronic neural implant", *Nature,* 2006, no. 444, pp. 56-60.

[30] N. Pourmand, M. Karhanek, H. H. J. Persson *et al.*, "Direct electrical detection of DNA synthesis", *PNAS*, 2006, no. 103, pp. 6466-6470.

[31] R. L. Fagaly, "Superconducting quantum interference device instruments and applications", *Rev. Sci. Instrum.*, 2006, no. 77, 101101 (45 pages).

[32] L. E. Fong, J. R. Holzer, K. K. McBride *et al.*, "High-Resolution Room-Temperature Sample Scanning Superconducting Quantum Interference Device Microscope Configurable for Geological and Biomagnetic Applications", *Rev. Sci. Instrum.*, 2005, no. 76, 053703-(1-9).

[33] N. Sinha, J. T.-W. Yeow, "Carbon Nanotubes for Biomedical Applications", *IEEE Trans. Nanobiosc.*, 2005, no. 4, pp. 180-195.

[34] D. S. Hopkins, D. Pekker, P. M. Goldbart *et al.*, "Quantum Interference Device Made by DNA Templating of Superconducting Nanowires", *Science*, 2005, no. 308, pp. 1762-1765.

[35] E. Vogel, "Technology and metrology of new electronic materials and devices", *Nature Nanotechnology*, 2007, no. 2, pp. 25-32.

[36] J. F. Jiang, Q. Y. Cai, H. M. Jiang *et al.*, "High-performance complementary metal-oxide-superconductor field effect transistor (CMOSuFET) current-mode operational amplifier", *Supercond. Sci. Technol.*, 1996, no. 9, pp. A66-A70.

[37] Sh. Suzuki, H. Tobisaka, and Sh. Oda, Electric properties of coplanar high-Tc superconducting field-effect devices, *Jpn. J. Appl. Phys.*, 1998, no. 37, Pt. 1, pp. 492-495.

[38] B. Yu, M. Meyyappan, "Nanotechnology: role in emerging nanoelectronics", *Solid-State Electronics*, 2006, no. 50, pp. 536-544.

[39] J. H. Schön, Ch. Kloc, and B. Batlogg, "High-temperature superconductivity in lattice-expanded C60", *Science*, 2001, no. 293, pp. 2432-2434.

[40] J. H. Schön, H. Meng, and Z. Bao, "Field-effect modulation of the conductance of single molecules", *Science*, 2001, no. 294, pp. 2138-2141.

[41] K. Nakamura, M. Ichikawa, R. Fushiki *et al.*, "Organic field-effect transistor of (thiophene/phenylene) co-oligomer single crystals with bottom-contact configuration", *Jpn. J. Appl. Phys.*, 2004, no. 43, pp. L100-L102.

[42] T. Jung, B. Yoo, L. Wang *et al.*, "Nanoscale n-channel and ambipolar organic field-effect transistors", *Appl. Phys. Lett.*, 2006, no. 88, 183102 (3 pages).

[43] J. A. Garrido, C. E. Nebel, and R. Todt, "Fabrication of in-plane gate transistors on hydrogenated diamond surfaces", *Appl. Phys. Lett.*, 2003, no. 82, pp. 988-1000.

[44] P. Avouris, J. Appenzeller, R. Martel *et al.*, "Carbon nanotube electronics", *Proc. of the IEEE*, 2003, no. 1772-1784.

[45] F. Nihey, H. Hongo, Y. Ochiai et al., "Carbon-nanotube field-effect transistors with very high intrinsic trans-conductance", *Jpn. J. Appl. Phys.*, 2003, no. 42, Pt. 2, L1288-L1291.

[46] Z. Zhong, D. Warmg, and Y. Cui, "Nanowire crossbar arrays as address decoders for integrated nanosystems", *Science*, 2003, no. 302, pp. 1377-1379.

[47] K. Keren, R. Berman, E. Buchstab *et al.*, "DNA-templated carbon nanotube field-effect transistor", *Science*, 2003, no. 302, pp. 1380-1382.

[48] G. Stix, "Nano Patterning", *Scientific American*, February 2004.

[49] S. Rosenblatt, Y. Yaish, J. Park *et al.*, "High performance electrolyte gated carbon nanotube transistors", *Nano Lett.*, 2002, no. 2, pp. 869-872.

[50] O. V. Lounasmaa, J. Knuutila, R. Salmelin, SQUID Technology and Brain Research, *Physica B*, 1994, no. 197, pp. 54-63.

[51] E. R. Flynn, "Factors Which Affect Spatial Resolving Power in Large Array Biomagnetic Sensors", *Rev. Sci. Instrum.*, 1994, no. 65, pp. 922-935.

[52] M. Bick, K. E. Leslie, R. A. Binks *et al.*, "Axial high-temperature superconducting gradiometer with a flexible flux transformer", *Applied Physics Letters*, 2004, no. 84, pp. 5347-5349.

[53] M. Voelker, P. Fromherz, "Nyquist Noise of Cell Adhesion Detected in a Neuron-Silicon Transistor", *Physical Review Letters*, 2006, no. 96, 228102 (4 pages).

[54] F. Patolsky, B. P. Timko, G. Yu *et al.*, "Detection, Stimulation, and Inhibition of Neuronal Signals with High-Density Nanowire Transistor Arrays", *Science*, 2006, no. 313, pp. 1100-1104.

[55] K. T. Ng *et al.*, "Noise and sensitivity analysis for miniature e-field probes", *IEEE Trans. Instrum. Meas.*, 1989, no. 30, pp. 27-31.

[56] H. Itozaki *et al.*, "Multi-channel high Tc SQUID", *IEICE Trans. on Electron.*, 2160 E77-C (1994), 1185-1190. (Invited paper)

[57] O. V. Lounasmaa *et al.*, SQUID technology and brain research, *Physica B* 197 (1994) 54-63.

[58] A. Sharma and K. R. Rogers, "Biosensors, *Meas. Sci. Technol.*, 1994, no. 5, pp. 461-472.

[59] G. L. Romani, S. J. Williamson, and L. Kaufman, "Biomagnetic instrumentation", *Rev. Sci. Instrum.*, 1982, no. 53, pp. 1815-1845.

[60] B. P. Helmke, A. R. Minerick, "Designing a nano-interface in a microfluidic chip to probe living cells: Challenges and perspectives", *PNAS*, 2006, no. 103, pp. 6419-6424.

[61] S. Meyburga, M. Goryllb, J. Moersb *et al.*, "N-channel field-effect transistors with floating gates for extracellular recordings", *Biosens. Bioelectr.*, 2006, no. 21, pp. 1037-1044.

[62] Ph. G. Collins, M. S. Arnold, and Ph. Avouris, "Engineering carbon nanotubes and nanotube circuits using electrical breakdown", Science, 2001, no. 292, pp.706-709.

[63] B. A. Korgel, "Materials science: self-assembled nanocoils", *Science*, 27th February 2004, no. 303, pp. 1308-9.

[64] R. C. Black, F. C. Wellstood, E. Dantsker *et al.*, "Eddy Current Microscopy Using a 77-K Superconducting Sensor", *Appl. Phys. Lett.*, vol. 64, 1994, issue 1, pp. 100-102.

[65] K. Nikawa, T. Kobayashi, K. Tanabe *et al.*, "Recent Topics in High-Tc Superconductive Electronics" (Invited Review Paper), *Jpn. J. Appl. Phys.* 44 (2005) 7735-7749.

[66] D. Read, I. Terry, S. R. Giblin, "Low Temperature Magnetic Susceptometer Based Upon a DC Superconducting Quantum Interference Device", *Rev. Sci. Instrum.* 77 (2006) 103906 (3 pages).

[67] R. C. Black, F. C. Wellstood, E. Dantsker *et al.*, "Microwave Microscopy Using a Superconducting Quantum Interference Device", *Appl. Phys. Lett.*, vol. 66, 1995, issue 1, pp. 99-101.

[68] T. J. Jackson, M. N. Keene, C. E. Gough, "A SQUID Magnetometer for Low Field DC Magnetization and AC Susceptibility Measurements", *Meas. Sci. Technol.*, 1992, no. 3, pp. 988-991.

[69] C. H. Barbosa, "Localization of Firearm Projectiles in the Human Body Using a Superconducting Quantum Interference Device Magnetometer: A Theoretical Study", *Rev. Sci. Instrum.*, vol. 75, 2004, issue 6, pp. 2098-2106.

[70] M. Gross, D. Altpeter, T. Stieglitz *et al.*, "Micromachining of flexible neural implants with low- ohmic wire traces using electroplating", *Sens. Act. A: Physical,* vol. 96, 2002, no. 2, pp. 105-110.

[71] K. C. Cheunga, Ph. Renaudb, "BioMEMS for medicine: on-chip cell characterization and implantable microelectrodes", *Solid-State Electronics*, vol. 50, 2006, issue 4, pp. 551-557.

[72] E. Arzt, S. Gorb, and R. Spolenak, "From micro to nano contacts in biological attachment devices, *PNAS*, 2003, no. 100, pp. 10603-10606.

[73] R. G. Ellis-Behnke, Y.-X. Liang, S.-W. You *et al.*, "Nano neuro knitting: peptide nanofiber scaffold for brain repair and axon regeneration with functional return of vision", *PNAS*, 2006, no. 103, pp. 5054-5059.

[74] A. V. Liopo, M. P. Stewart, J. Hudson *et al.*, "Biocompatibility of native and functionalized single-walled carbon nanotubes for neuronal interface", *Journal. of Nanoscience and Nanotechnol.*, vol. 6, 2006, no. 5, pp. 1365-1374.